Active beating of a reconstituted synthetic minimal axoneme

Isabella Guido,[1,*] Andrej Vilfan,[1,2] Kenta Ishibashi,[3,4] Hitoshi Sakakibara,[5] Misaki Shiraga,[6] Eberhard Bodenschatz,[1,7,8] Ramin Golestanian,[1,9,†] and Kazuhiro Oiwa[5,6]

[1]*Max Planck Institute for Dynamics and Self-Organization (MPIDS), 37077 Göttingen, Germany*
[2]*Jožef Stefan Institute, 1000 Ljubljana, Slovenia*
[3]*Graduate School of Frontier Biosciences, Osaka University, Osaka 5650871, Japan*
[4]*Center for Information and Neural Networks (CiNet), National Institute of Information and Communications Technology, Osaka 565-0871, Japan*
[5]*Advanced ICT Research Institute, National Institute of Information and Communications Technology, Kobe 651-2492, Japan*
[6]*Graduate School of Life Science, University of Hyogo, Hyogo 678-1297, Japan*
[7]*Institute for Dynamics of Complex Systems, Georg-August-University Göttingen, 37073 Göttingen, Germany*
[8]*Laboratory of Atomic and Solid-State Physics, Cornell University, Ithaca, NY 14853, United States*
[9]*Rudolf Peierls Centre for Theoretical Physics, University of Oxford, Oxford OX1 3PU, United Kingdom*

Propelling microorganisms through fluids and moving fluids along cellular surfaces are essential biological functions accomplished by long, thin structures called motile cilia and flagella, whose regular, oscillatory beating breaks the time-reversal symmetry required for transport. Although top-down experimental approaches and theoretical models have allowed us to broadly characterize such organelles and propose mechanisms underlying their complex dynamics, constructing minimal systems capable of mimicking ciliary beating and identifying the role of each component remains a challenge. Here we report the bottom-up assembly of a minimal synthetic axoneme, which we call a synthoneme, using biological building blocks from natural organisms, namely pairs of microtubules and cooperatively associated axonemal dynein motors. We show that upon provision of energy by ATP, microtubules undergo rhythmic bending by cyclic association-dissociation of dyneins. Our simple and unique beating minimal synthoneme represents a self-organized nanoscale biomolecular machine that can also help understand the mechanisms underlying ciliary beating.

INTRODUCTION

Eukaryotic cilia and flagella accomplish vital physiological tasks [1, 2], ranging from the swimming and feeding of microorganisms to the clearance of mucous in airways [3], establishment of left-right body asymmetry and transport of cerebrospinal fluid in brain ventricles [4] and the spinal cord. Defects in ciliary assembly or in their function are responsible for diseases that affect millions of patients worldwide [5]. Each cilium's structural framework is the axoneme, which consists of nine microtubule doublets and several hundred other proteins that maintain its structure, drive and control the beat, and transport the materials [6]. The beating is powered by axonemal dyneins that form two arrays (outer and inner dynein arms) along the side wall of the doublet microtubules. They generate interdoublet shear that causes the bending of microtubule doublets [7].

The analysis of *Chlamydomonas* flagellar mutants [8], biochemical and biophysical [9] identification and structural studies [10], especially using cryoelectron tomography [7], have progressed our understanding on the molecular organization and function of each axonemal component [11]. Recently, axonemal dyneins have been reported to have mechanical and structural properties so distinct from other protein motors to be suitable for the fabrication of biomolecular nanomachine [12, 13].

How this complex structure drives the beating patterns is not yet well understood [11, 14–18]. A controlled assembly of minimal systems that reproduce certain aspects of ciliary dynamics with far less cellular feedback mechanisms can be an important step towards solving the puzzle of ciliary beating dynamics. To address this issue we use the bottom-up approach and reconstitute in-vitro a minimal axoneme made of the main axonemal constituents, outer dynein arms (ODA) and microtubules, and we reproduce the bending oscillation of the natural cilia (flagella). We call this structure a "synthoneme" in analogy to the the well described axoneme.

The modularity of the reconstituted structure of this synthoneme, its defined geometry and the nature of the building blocks allow the system to go beyond the minimal beating systems reported in the past. Namely, two microtubule doublets extended from frayed and disintegrated axonemes that exhibit repetitive buckling [19, 20]; mixtures of microtubule bundles and kinesin-1 clusters, which self-assemble in cilia-like beating structures [21, 22]. The controlled assembly of our synthoneme has the potential for the development of controllable beating structures that can serve as a tool for the understanding of the flagellar/ciliary beating and for eventual technological advance in the field of bio-inspired systems.

RESULTS

The reconstituted minimal bending system is made of taxol-stabilized microtubules and ODA extracted from flagella of the green algae *Chlamydomonas reinhardtii* (See Supplementary Fig. S1). We chose to use ODA for its ability to self-organize in arrays on microtubules [23], the high yield in preparation, and its robust motility *in vitro* [8, 24, 25].

Microtubules are polymerized in an experimental chamber by flowing porcine brain tubulin over fragmented *Chlamydomonas* axonemes (hereafter named seeds). The seeds repre-

sent the joint basal end of the microtubule pair and are spontaneously attached to the coverslip. This heterologous seeding procedure provides microtubule pairs with the same polarity in which the filaments grow at a distance on axoneme scale. With the seeds the relative movement of microtubules is blocked at the basal end of the pair, but free at the distal end.

These properties allow the repetitive buckling of the microtubules driven by dynein. The distance between two polymerized microtubule singlets at the basal end probably ranges from the minimal distance between two A-tubules of adjacent doublets (approx. 30 nm) and the maximum corresponding to the diameter of the axoneme (approx. 200 nm) (see Supplementary Fig. S2). Since the length of microtubules is longer than 10 μm, the tips of the filaments thermally fluctuated unless ODAs formed cross-bridges between them. Therefore, a precise determination of the inter-microtubule distance in individual cases is not applicable in our observations.

The ODA is provided to the system by perfusion of extract from axonemes containing ODAs and ODA-docking complex (ODA-DC) into the flow chamber. Due to the presence of the docking complex, ODAs are associated with the microtubule with high cooperativity in an end-to-end fashion and thereby align unidirectionally along one protofilament [23]. We confirm the reconstitution of ODAs on microtubules with negative staining electron microscopy (Fig. 1A and Supplementary Fig. S3) and the longitudinal 24-nm periodicity of ODA/ODA-DC aligned along the filament is identified by Fourier analysis (Fig. 1B). This periodicity is characteristic for ODAs in native axonemes [7] and reconstituted ODAs systems shown in previous studies [26].

The EM images and subsequent analysis also provide information about the occupancy of dynein arrays on microtubules (see SI text and Figs. S3 and S4 for more details). At high mixing ratios ODA arrays occupy most of microtubules and the length of the arrays are probably underestimated due to the limited size of the observation field. However, the length distribution of contiguous dynein arrays shows that the average length of about $\sim 200\,\mathrm{nm}$ (corresponding to approx. eight ODAs) is largely independent of the mixing ratio (Fig. 1C). We concluded that the ODA alignment is a highly cooperative assembly process.

After adding 1mM Mg–ATP to the system we observe many microtubule pairs with a joint basal end bending persistently We explain the functional mechanism behind the observation in the following way. Free microtubule ends fluctuate in the bulk. Dynein motors assembled on one microtubule attach to the adjacent microtubule, then Brownian fluctuations are suppressed. By using energy from ATP hydrolysis, the motors cooperatively produce shearing forces between these two microtubules (see Fig. 2A). When they reach the buckling instability, the filaments separate.

In more detail, one microtubule slides towards the seed. When the crossing angle between the microtubules increases, the forces on the motors increase and thus an increasing number of motors detaches without the possibility to rebind. The other microtubule bends only weakly. The motion is stalled when the force produced by the remaining motors reaches the force of the buckled microtubules. After that, stochastic fluctuations can tip the motors into cooperative detachment, akin to a catastrophic failure, which leads to a fast straightening of the microtubules and a return to the original state. The straight microtubules again allow the attachment of a larger number of motors. We observed that this process could repeat itself periodically. This cycle and the functional mechanism are illustrated in the schematic representation in Fig. 2B.

The long lag phase and subsequent rapid sliding leading to rapid buckling indicate that the attachment and movement of motors take place in a cooperative manner, too. The simplest possible explanation is that the attachment rate of the first motor between unconnected microtubules is low because of thermal fluctuations. The first motor capturing the adjacent microtubule then suppresses the fluctuations and largely accelerates the attachment of subsequent motors. The mechanism in which microtubule buckling accelerates the detachment of motors is also at the core of the geometric clutch hypothesis for ciliary beating [15]. On the other hand, the release of the motors under load is reminiscent of models that propose a dynamic instability in the sliding motion between microtubule doublets [27].

We quantify the oscillations by measuring the maximal distance H between the buckled microtubules. A typical time series representing the bending cycle is shown in Fig. 3A. This cycle can be divided into four phases consisting of an active bent state and a relaxed state with variable duration and the two transitions between them, namely a rapid bending from the relaxed to the active state and a rapid unbending from the active to the relaxed state. The four phases are influenced also by the stochastic nature of dynein motors. Both rapid bending and unbending phases completed within a few hundred milliseconds. The swiftness of the transitions is a likely clue on the cooperativity of the motors as the motor recruitment acts collectively to transition between states.

By analyzing the histogram of distances H in Fig. 3B we can observe a bimodal distribution. Therefore, the above description of the bending cycle as a process with two states is a suitable one. We will call them *open* and *close*, and consider stochastic transitions between them. We denote the rates of the closed-open and open-closed transition with k_+ and k_-, respectively. The discretized variable H then has the character of a telegraph noise process. A robust way to determine the two rate constants is from the occupancy ratio ($P_{\mathrm{open}}/P_{\mathrm{closed}} = k_+/k_-$) and from the autocovariance function of H, which for the telegraph process has the dependence $\sim \exp(-(k_+ + k_-)\tau)$. The autocovariance functions are shown in Fig. 3C. They have a bi-exponential form – besides the slow component, related to the open/closed transitions, a fast one resulting from noise with a short correlation time. From the slow rate and $P_{\mathrm{open}}/P_{\mathrm{closed}} = 1.7 \pm 0.5$, we obtain the rates $k_+ = (0.18 \pm 0.07)\,\mathrm{s}^{-1}$ and $k_- = (0.10 \pm 0.04)\,\mathrm{s}^{-1}$.

We use the elastic model that is described in the next section to estimate the force and the energy needed to buckle

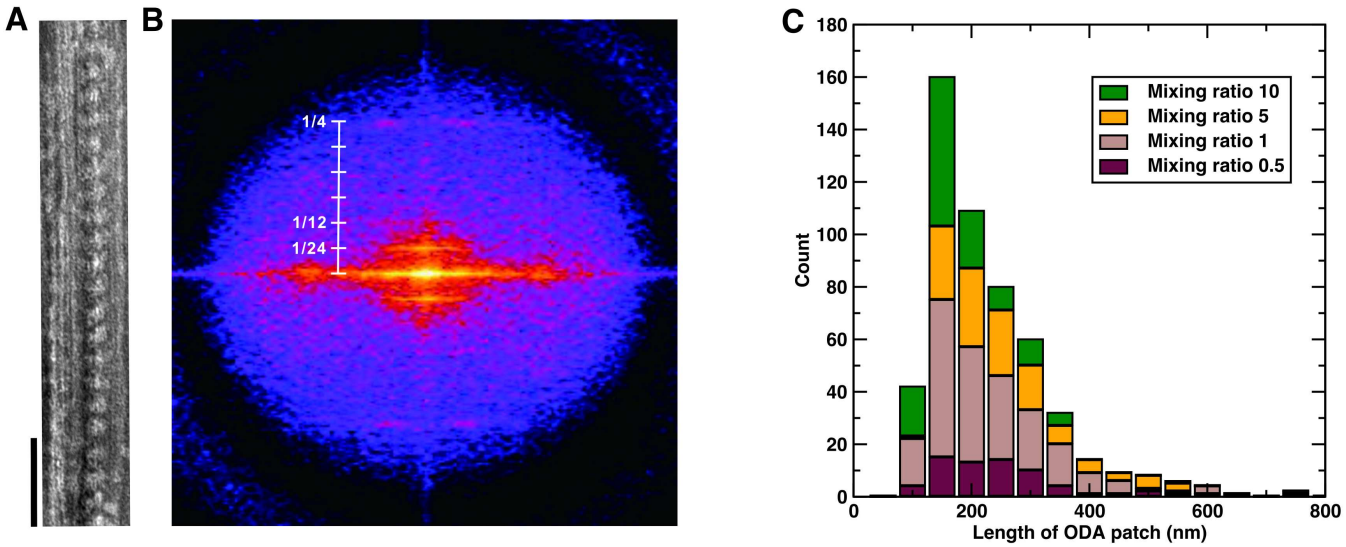

FIG. 1. A) Negative staining EM image showing a portion of a microtubule microtubule and an assembly of the ODA complex. Globular blobs are regularly aligned along the microtubule. Scale bar: 100 nm. B) Fourier transform of EM images shows a 24 nm periodicity of ODA on microtubules. 1/4 nm^{-1} layer lines derived from microtubules are clearly observed (scale unit: 1/24 nm^{-1}). C) Length distribution of ODA patches at different mixing ratios between ODA and microtubules. The peak length is around 100–200 nm irrespective of the mixing ratio.

the filaments. With a typical length of $l = 8\,\mu$m and $EI = 4 \times 10^{-24}\mathrm{Nm}^2$, Eq. (2) gives $F \approx 1\,$pN, showing that a small number of dyneins is sufficient to buckle the filaments. For a typical distance $H = 1.2\,\mu$m, we further calculate the elastic energy of the buckled state as $F\Delta s \approx 480 \times 10^{-21}\mathrm{Nm} \approx 116\,k_BT$. Changes in elastic energy that exceed the thermal energy by two orders of magnitude prove that the beating is actively driven by molecular motors, i.e., that we assembled an active system.

Theory and Simulation.

The shapes of the two bent filaments (Fig. 4A) and the forces that the dyneins need to produce to enter the bent configuration can be calculated by linear elasticity theory if we assume that the shape is quasi-static and that the deflections are small. In contrast to earlier models [28], we allow both filaments to bend. Because both ends are force-free, the force in filament 1 is exactly opposite to that in filament 2. The curvature in each filament is proportional to the local bending moment

$$EI\,y_i''(x) = F_i y_i(x)\,. \tag{1}$$

The resulting equation is solved with the ansatz $y_1 = A\sin kx$, $y_2 = B\sinh kx$ with $k = \sqrt{F/EI}$. The boundary condition at l leads to the equation $\tan kl = \tanh kl$ with the lowest non-trivial solution $kl = 3.9266$ and

$$F = 1.5622\frac{\pi^2 EI}{l^2}\,. \tag{2}$$

This equation can be used to estimate the force produced by the motors that is needed to buckle the filaments. Notably, the prefactor in the buckling load of 1.5622 lies between the values of 1 that applies to the classical Euler problem with two pinned ends and 2.046 for one pinned and one clamped end [29]. As expected, clamping one end to a flexible filament leads to a lower critical load than clamping it to a fixed direction in space.

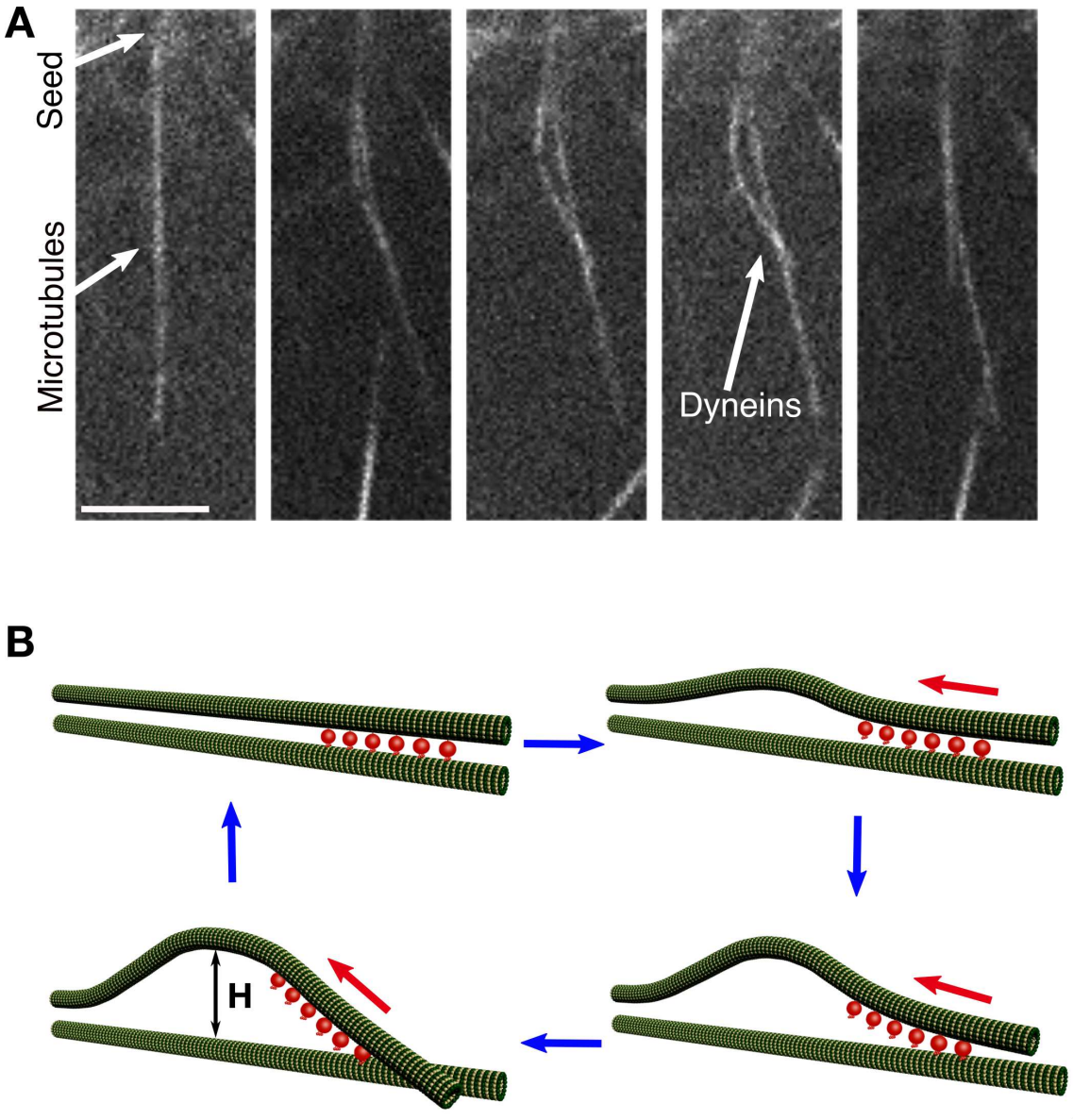

FIG. 2. A) Micrographs of bending cycle of two microtubules forming a synthoneme. Scale bar: 10 μm B) Schematic representation of the filament buckling. Initially, the filaments (green) are straight and the dynein motors (red) enter the active state. The force produced by the dyneins buckles the filament on which they are attached. The buckling changes the crossing angle between the microtubules, which reduces the number of dyneins that can bind to both of them.

The length difference between the filament segments, Δs, and the distance H can be derived as functions of the crossing angle φ (see SI).

Dynamical model. The behavior of the system over time observed during the experiments can be described by a dynamical model. The two filaments (each of length L) are clamped at the minus end (Fig. 4B). Filament 1 is bearing dynein motors between length L_0 and L, at a line density ρ. Each motor can be in the attached or detached state. Attachment can take place in the overlap zone $l_1 \pm d/\varphi$, where d is a characteristic distance between filaments that the motors can bridge. In that zone, the attachment rate of the motors is k_{on}. However, we use a lower constant k_{on}^0 for two reasons: (i) a reduced attachment rate for the motors that align end-to

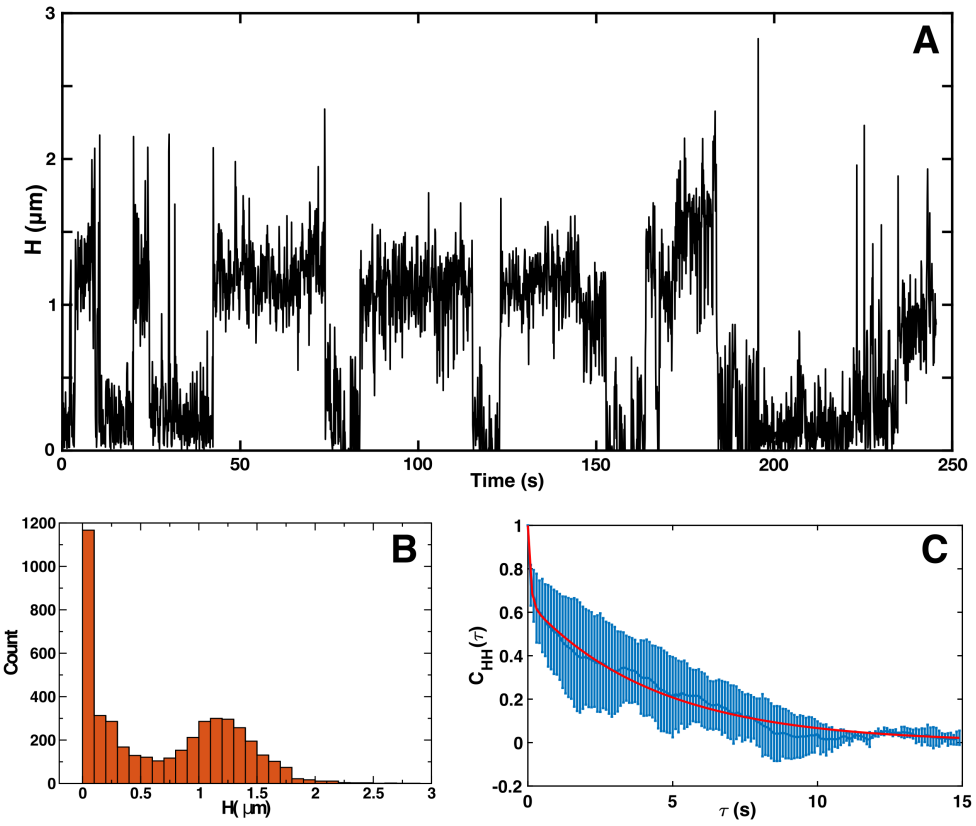

FIG. 3. A) Maximal distance between the filaments in the buckled region (H), as defined in Fig. 2, as function of time. B) Distribution of distances H between the filaments. As the distribution is clearly bimodal, we designated the two states as open and closed. C) Normalized autocovariance function $C_{HH}(\tau) = (\langle H(t+\tau)H(t)\rangle - \langle H\rangle^2)/\langle (H(t)-\langle H\rangle)^2\rangle$.

end along one filament indicates the cooperativity between the motors; (ii) the effective attachment rate is strongly reduced by thermal fluctuation when the motors are simultaneously in the detached state. For a motor loaded with force f we use a detachment rate $k_{\rm off} = k^0_{\rm off}\exp(\alpha f)$, where α is a parameter representing the inverse characteristic detachment force.

A motor attached on filament 1 with load f moves towards the minus end of filament 2 with velocity $v = {\rm d}(\Delta s)/{\rm d}t$ determined by a linear force-velocity relationship

$$f = f_s(1 - v/v_m) \tag{3}$$

with the parameters f_s (stall force) and v_m (unloaded velocity). When n motors are attached, they share the load equally such that $F(l_2) = nf$.

We explain the oscillatory cycle of the filaments observed in the experiments through the following stages: First, all motors are detached and the first attachment takes place randomly with the rate $k^0_{\rm on}$. This increases the binding rate of remaining motors to $k_{\rm on}$. After a short time, the total motor force nf_s surpasses the buckling force $F(l)$, where l is the distance to the first bound motor. The straight state becomes unstable. By considering the duty ratio of stalled motors (fraction of time spent in the attached state)

$$\eta = \frac{k_{\rm on}}{k_{\rm on} + k^0_{\rm off}\exp(\alpha f_s)}\,, \tag{4}$$

the condition of buckling is

$$\eta f_s \rho (L - L_0) > F(L_0) = 1.5622\frac{\pi^2 EI}{L_0^2}\,. \tag{5}$$

The initial buckling instability is followed by the growth of the bulge, driven by the sliding action of motors in the overlap zone. During this phase, the crossing angle φ increases, which reduces the length and the number of motors in the overlap zone, leading to a metastable state, where the force balance is reached at an angle φ when $\eta\rho f_s 2d/\varphi = F(l)$.

Through random detachment of motors, a "catastrophic failure" can take place when detachment of motors leads to an increased load on the remaining ones, further increasing

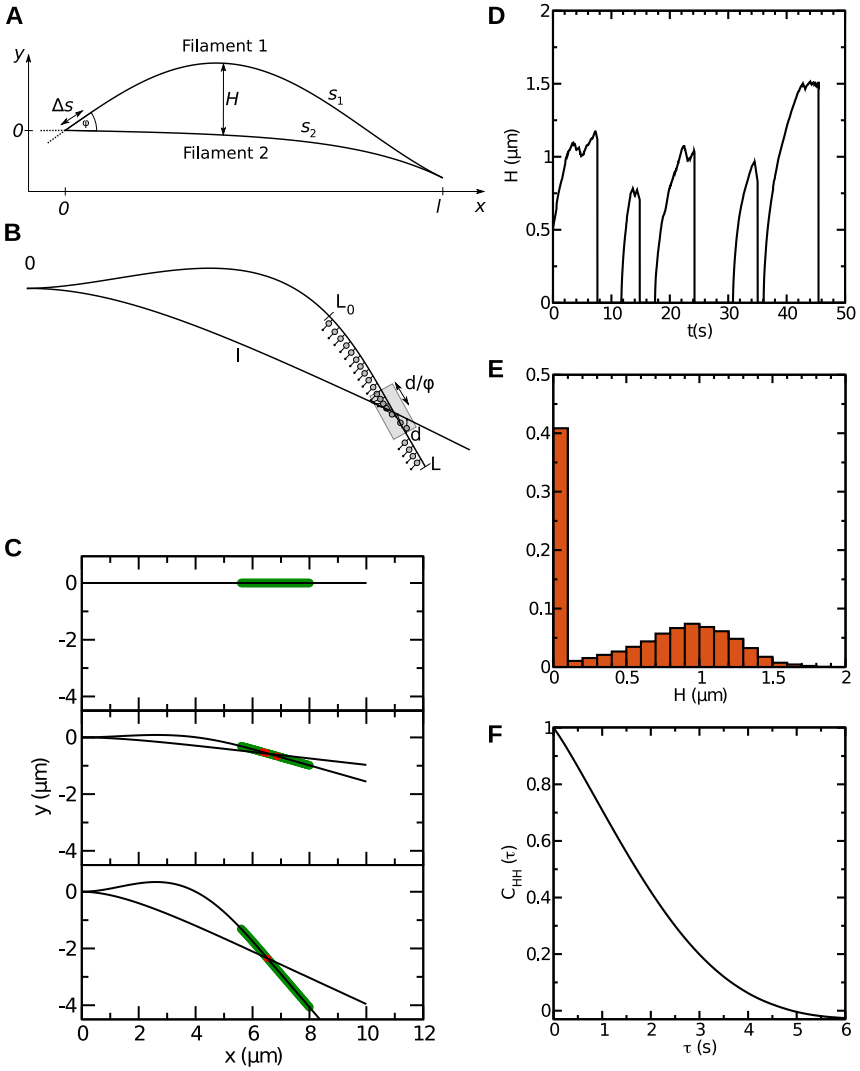

FIG. 4. Theoretical description of the active synthoneme. A) Elastic model. Two filament segments of different lengths are pinned to each other at $x = 0$ and clamped at $x = l$. They are parameterized with the functions $y_1(x)$ and $y_2(x)$. The x-axis represents the direction of the force. The condition for the pinned end at $x = 0$ is $y_1(0) = y_2(0) = 0$. At the clamped end, the condition is $y_1(l) = y_2(l)$ and $y_1'(l) = y_2'(l)$. B) Active model: two filaments are clamped in the origin. Filament 1 is decorated with motors from length L_0 to length L. Motors can bind to filament 2 if the distance between the filaments is smaller than d (grey rectangle). C) Snapshots from a stochastic simulation. The black lines show two filaments, red and green circles show bound and free motors, respectively. The upper panels shows the filaments before binding, the middle panel the onset of buckling and the lower panel a stalled state before catastrophic detachment of motors. D) The distance between the filaments H as a function of time from the simulation. E) Distribution of distances H from the simulation. As in the experiment, a strongly bimodal distribution is visible. F) Autocorrelation function of the distance H as a function of time.

their detachment rate. We assess the stability of a state with the following consideration. At a constant total force F, initially distributed over n attached motors, the on-off dynamics is given by the master equation

$$\dot{n} = (N-n)k_{\text{on}} - nk_{\text{off}}e^{\alpha F/n}. \tag{6}$$

Its stability is determined by the derivative

$$\frac{\partial \dot{n}}{\partial n} = -k_{\text{on}} + \left(\frac{\alpha F}{n} - 1\right) k_{\text{off}} e^{\alpha F/n} \tag{7}$$

which is positive when $\alpha f_s n_0/n > 1/(1-\eta)$. As a rough estimate, we expect an instability when $\alpha f_s \gtrsim 1$.

Through full detachment, the filaments finish in the straight position where new motors quickly re-attach and repeat the

cycle. This is compatible to the cyclic dynamics that we hypothesized for our experimental outcomes.

The elastic model and the motor model described above are combined in a stochastic simulation that confirms the experimental results (Fig. 4C-F). The distance between the filaments oscillates with steep transitions between the open and the closed state (Fig. 4D), closely resembling the experimental traces shown in Fig. 3A. The histogram of distances shows a clear bimodal distribution (Fig. 4E), as in the experimental data Fig. 3B. Finally, the autocorrelation function shows a near-exponential decay (Fig. 4F). In contrast with the experiment (Fig. 3C), the fast phase is missing as we did not include thermal noise and measurement uncertainty in the simulation.

CONCLUSION

The reconstituted minimal axoneme, i.e. the synthoneme, that we present in this study is a one-of-a-kind result resembling the natural system with its beating behavior. All crucial components of our synthoneme are assembled in-vitro in a bottom-up approach. We show that the cooperativity of the dynein motors to arranging on the filament as well as to actuating the buckling can be reconstituted in-vitro. Although the amplitude and frequency of oscillations are still well below those of natural cilia, we have shown that the basic functionality can be established with a far smaller number of proteins. Specifically, while cilia contain several hundred different proteins, our synthetic axoneme works with only three components (tubulin, ODA, ODA-DC). The observation that synthetic systems consisting only of molecular motors and filaments can reproduce the basic movement necessary for cilia/flagella beating also provides clues about the amount of complexity needed by the ancestor cilia to first achieve beating motility. Indeed, some organisms like the male gamete of the parasitic protozoan *Diplauxis hatti* have a motile axoneme with only three doublets instead the classical "9 + 2" structure [30]. This suggests that bending behavior could be produced by simpler structures that have filaments and motors. Future refinements will lead to a convergence between the synthetic and the natural cilium. This will provide a systematic way of dissecting the elusive beating mechanism.

Besides the potential of this system for answering important questions about ciliary beating, our synthetic cilium may encourage the technological development of molecular machines for fluid transport at micro- and nanoscale. Most previous attempts to build artificial cilia have concentrated on magnetic [31, 32], electrostatic [33] or optical [34] actuation mechanisms to produce motion similar to the natural one. These studies showed hydrodynamic entrainment between adjacent structures and creation of metachronal waves. However, these systems are unrelated to biological cilia. In the future our system will also be developed as multi-cilia system by using axoneme seeds as the base and aligning them and we will achieve the synchronization of axonemal beating.

MATERIALS AND METHODS

Preparation of the crude dynein extract

Demembranated axonemes are suspended in 0.6M KCl containing HMDEK solution to extract crude dynein sample (see SI for more details about preparation). After spinning down the axonemes for 5 min, the supernatant is desalted with the overnight dialysis against HMDEK solution (Spectra/Por Dialysis Membrane, MWCO:100-500D, Biotech CE). The concentration of the crude dynein extract is measured with Bradford method and the concentration used during the experiments was 0.02 mg/ml.

Preparation of dynein–MT complexes

The flow chamber was build with Teflon-treated coverslips as previously described in [35] and spaced with double-coated tape (80mm thick, W-12; 3M, St. Paul, MN) to prevent any nonspecific binding of proteins onto the surface. Microtubules growing close to each other and with the same polarity were obtained by using fragments of demembranated axonemes prepared by rigorous pipetting as polymerization seeds. The ODA–MT complexes are reconstituted in the flow cell by flowing the components one after the other. Briefly, in the flow cell a small amount of axonemes are attached on the bottom of the flow cell. After 5-min incubation, the flow cell is washed with 1% (w/v) Pluronic® F127 in BRB80 (80 mM PIPES, 1 mM $MgCl_2$, 1 mM EGTA, pH 6.8 with KOH) and is incubated for 5 min. After washing the chamber with BRB80, fluorescently-labeled (Cy3–labeled) porcine tubulin (3% labeling) is introduced into the flow cell, polymerized in the presence of 1 mM GTP, 50% DMSO, 1mM $MgCl_2$ at 37°C for 30 min and stabilized with 7 μM taxol. After microtubule polymerization, diluted crude-dynein extract is introduced into the flow cell and incubated for 5 min. The non-bound protein is eliminated by washing the chamber with buffer and afterwards 1mM ATP is perfused into the chamber to trigger the activity.

Imaging and tracking

Fluorescence images of the MT-ODA complex are acquired using an inverted fluorescence microscope Ti-E (Nikon, Japan) equipped with a 60× CFI Apochromat objective (N.A.=1.49, Nikon, Japan) and the confocal unit (CSU-X1, YOKOGAWA, Japan). The data is recorded with an iXon Ultra EMCCD camera (Andor Japan, Japan). The images are acquired at a frequency of 10 Hz. The movement of the filaments over times was tracked manually and a third order polynomial was fitted to the data by using a purpose-written MATLAB code.

Acknowledgements E.B., I.G., and R.G. acknowledge support from the MaxSynBio Consortium which is jointly

funded by the Federal Ministry of Education and Research of Germany and the Max Planck Society. E.B. acknowledges support from the Volkswagen Stiftung (priority call "Life?"). A.V. acknowledges support from the Slovenian Research Agency (grant no. P1-0099). K.O. acknowledges MEXT/JSPS KAKENHI, grant numbers 26440089, 17K07376 and JP16H06280, the Takeda Science Foundation and Hyogo Science and Technology Association that partly supported the project.

* isabella.guido@ds.mpg.de
† ramin.golestanian@ds.mpg.de

[1] Satir, P. & Christensen, S. T. Overview of structure and function of mammalian cilia. *Annu. Rev. Physiol.* **69**, 377–400 (2007).
[2] Gilpin, W., Bull, M. S. & Prakash, M. The multiscale physics of cilia and flagella. *Nat. Rev. Phys.* **2**, 74–88 (2020).
[3] Loiseau, E. *et al.* Active mucus–cilia hydrodynamic coupling drives self-organization of human bronchial epithelium. *Nat. Phys.* **16**, 1158–1164 (2020).
[4] Faubel, R., Westendorf, C., Bodenschatz, E. & Eichele, G. Cilia-based flow network in the brain ventricles. *Science* **353**, 176–178 (2016).
[5] Fliegauf, M., Benzing, T. & Omran, H. When cilia go bad: cilia defects and ciliopathies. *Nat. Rev. Mol. Cell Biol.* **8**, 880–893 (2007).
[6] Ishikawa, T., Sakakibara, H. & Oiwa, K. The architecture of outer dynein arms in situ. *J. Mol. Biol.* **368**, 1249–1258 (2007).
[7] Lin, J. & Nicastro, D. Asymmetric distribution and spatial switching of dynein activity generates ciliary motility. *Science* **360** (2018).
[8] Kamiya, R. & Yagi, T. Functional diversity of axonemal dyneins as assessed by in vitro and in vivo motility assays of Chlamydomonas mutants. *Zoolog. Sci.* **31**, 633–644 (2014).
[9] Sakakibara, H., Kojima, H., Sakai, Y., Katayama, E. & Oiwa, K. Inner-arm dynein c of chlamydomonas flagella is a single-headed processive motor. *Nature* **400**, 586–590 (1999).
[10] Burgess, S. A., Walker, M. L., Sakakibara, H., Knight, P. J. & Oiwa, K. Dynein structure and power stroke. *Nature* **421**, 715–718 (2003).
[11] Mitchison, T. J. & Mitchison, H. M. How cilia beat. *Nature* **463**, 308–309 (2010).
[12] Sumino, Y. *et al.* Large-scale vortex lattice emerging from collectively moving microtubules. *Nature* **483**, 448–452 (2012).
[13] Furuta, A. *et al.* Creating biomolecular motors based on dynein and actin-binding proteins. *Nat. Nanotechnol.* **12**, 233–237 (2017).
[14] Sartori, P., Geyer, V. F., Scholich, A., Jülicher, F. & Howard, J. Dynamic curvature regulation accounts for the symmetric and asymmetric beats of Chlamydomonas flagella. *eLife* **5**, e13258 (2016).
[15] Lindemann, C. B. A "geometric clutch" hypothesis to explain oscillations of the axoneme of cilia and flagella. *J. Theor. Biol.* **168**, 175–189 (1994).
[16] Lindemann, C. B. & Lesich, K. A. Flagellar and ciliary beating: the proven and the possible. *J. Cell Sci.* **123**, 519–528 (2010).
[17] Geyer, V. F., Sartori, P., Friedrich, B. M., Jülicher, F. & Howard, J. Independent control of the static and dynamic components of the Chlamydomonas flagellar beat. *Curr. Biol.* **26**, 1098–1103 (2016).
[18] Sartori, P., Geyer, V. F., Howard, J. & Jülicher, F. Curvature regulation of the ciliary beat through axonemal twist. *Phys. Rev. E* **94**, 042426 (2016).
[19] Kamiya, R. & Okagaki, T. Cyclical bending of two outer-doublet microtubules in frayed axonemes of Chlamydomonas. *Cell Motil.* **6**, 580–585 (1986).
[20] Aoyama, S. & Kamiya, R. Cyclical interactions between two outer doublet microtubules in split flagellar axonemes. *Biophys. J.* **89**, 3261–3268 (2005).
[21] Sanchez, T., Welch, D., Nicastro, D. & Dogic, Z. Cilia-like beating of active microtubule bundles. *Science* **333**, 456–459 (2011).
[22] Vilfan, A., Subramani, S., Bodenschatz, E., Golestanian, R. & Guido, I. Flagella-like beating of a single microtubule. *Nano Lett.* **19**, 3359–3363 (2019).
[23] Owa, M. *et al.* Cooperative binding of the outer arm-docking complex underlies the regular arrangement of outer arm dynein in the axoneme. *Proc. Natl. Acad. Sci. U.S.A.* **111**, 9461–9466 (2014).
[24] Furuta, A., Yagi, T., Yanagisawa, H., Higuchi, H. & Kamiya, R. Systematic comparison of in vitro motile properties between Chlamydomonas wild-type and mutant outer arm dyneins each lacking one of the three heavy chains. *J. Biol. Chem.* **284**, 5927–5935 (2009).
[25] Seetharam, R. N. & Satir, P. Coordination of outer arm dynein activity along axonemal doublet microtubules. *Cell Motil.* **65**, 572–580 (2008).
[26] Oda, T., Hirokawa, N. & Kikkawa, M. Three-dimensional structures of the flagellar dynein-microtubule complex by cryoelectron microscopy. *J. Cell Biol.* **177**, 243–252 (2007).
[27] Camalet, S., Jülicher, F. & Prost, J. Self-organized beating and swimming of internally driven filaments. *Phys. Rev. Lett.* **82**, 1590–1593 (1999).
[28] Brokaw, C. J. Simulation of cyclic dynein-driven sliding, splitting, and reassociation in an outer doublet pair. *Biophys. J.* **97**, 2939–2947 (2009).
[29] Gere, J. & Goodno, B. *Mechanics of Materials* (Cengage Learning, 2012).
[30] Prensier, G., Vivier, E., Goldstein, S. & Schrevel, J. Motile flagellum with a "3 + 0" ultrastructure. *Science* **207**, 1493–1494 (1980).
[31] Vilfan, M. *et al.* Self-assembled artificial cilia. *Proc. Natl. Acad. Sci. U.S.A.* **107**, 1844–1847 (2010).
[32] Dong, X. *et al.* Bioinspired cilia arrays with programmable nonreciprocal motion and metachronal coordination. *Sci. Adv.* **6**, eabc9323 (2020).
[33] den Toonder, J. *et al.* Artificial cilia for active micro-fluidic mixing. *Lab Chip* **8**, 533 (2008).
[34] van Oosten, C. L., Bastiaansen, C. W. M. & Broer, D. J. Printed artificial cilia from liquid-crystal network actuators modularly driven by light. *Nat. Mater.* **8**, 677–682 (2009).
[35] Torisawa, T., Taniguchi, D., Ishihara, S. & Oiwa, K. Spontaneous formation of a globally connected contractile network in a microtubule-motor system. *Biophys. J.* **111**, 373–385 (2016).
[36] Kagami, O. & Kamiya, R. Translocation and rotation of microtubules caused by multiple species of Chlamydomonas inner-arm dynein. *J. Cell Sci.* **103**, 653–664 (1992).
[37] Witman, G. B., Plummer, J. T. & Sander, G. Chlamydomonas flagellar mutants lacking radial spokes and central tubules. structure, composition, and function of specific axonemal components. *J. Cell Biol.* **76**, 729–47 (1978).
[38] Haimo, L. T., Telzer, B. R. & Rosenbaum, J. L. Dynein binds to and crossbridges cytoplasmic microtubules. *Proc. Natl. Acad. Sci. U.S.A.* **76**, 5759–5763 (1979).

SUPPLEMENTARY MATERIALS AND METHODS

Preparation of *Chlamydomonas reinhardtii*. Axonemes and their demembranation.

Axonemes were obtained from *Chlamydomonas reinhardtii* according to the dibucaine method [36, 37]. *C. reinhardtii* wild type strain (137c mt-) and the outer-arm less mutant (*oda1*) were cultured in 4 liters of the liquid TAP medium under continuous illumination at 20 °C for 4 days with air bubbling. Cells were harvested by centrifugation at 1692×g (3000 rpm, R10A3 rotor, Himac CR22E) for 6 min, and then re-suspended in 40 ml ice-cold HMDS (30 mM HEPES-NaOH, 5 mM $MgSO_4$, 1 mM dithiothreitol (DTT), 4% sucrose, pH 7.4). All procedures described below were conducted at 4 °C or on ice unless otherwise stated. The cell suspension was moved to a 50-ml conical centrifuge tube and 2.5 mM (final concentration) dibucaine HCl (Wako, 167-15111) was added. The suspension was pipetted rapidly in and out of 10-ml Falcon disposable plastic pipettes for 30 s. Afterwards 200 μl of 100 mM EGTA was added and the solution was gently resuspended several times. The cell bodies were removed by centrifugation at 1670×g (3000 rpm, RS-4 rotor, KUBOTA 6800) for 6 min, the supernatant was transferred to a new 50-ml conical centrifuge tube and centrifuged again as above. The cell-free supernatant was centrifuged at 27720×g (15,000 rpm, RSR20-2 rotor Himac CR21) for 12 min. The resulting pellet was resuspended in 1.5 ml of HMDEK (30 mM HEPES-NaOH, 5 mM $MgSO_4$, 1 mM DTT, 1 mM EGTA, 50 mM potassium-acetate, pH 7.4) and demembranated by adding 15 μl of 20% Nonidet P-40 (NP-40, Nacalai Tesque). After 5 min-incubation, the suspension was centrifuged at 21130×g (15,000 rpm, FA-45-24-11 rotor, Eppendorf 5452R) for 5 min, and resuspended in 1.5 ml HMDEK. This procedure was repeated twice to remove detergent. Axonemes were collected by centrifugation as described above. An aliquot of the demembranated *oda1* axonemes was used to prepare the seeds of microtubule polymerization. Suspension of the axonemes was gently homogenized with a Teflon pestle and pipetting. The resultant suspension was centrifuged at 3380×g at 4 °C for 10 min. The pellet was resuspended with a small amount of HMEDK solution. Intrinsic dyneins of the seeds were deactivated and the sliding among doublet microtubules was inhibited with the treatment of ethylene glycol bis(succinimidyl succinate) (Thermo Fisher Scientific, 21565).

Preparation of of the crude dynein extract.

For the extraction of ODAs and docking complex from the *Chlamydomonas reinhardtii* wild-type axonemes we follow the method described in previous works [20, 38]. As reference, we prepared high-salt extract from *oda1* (outer-arm less mutant) axonemes. Demembranated axonemes were resuspended in 0.6M KCl containing HMDEK solution to extract crude dynein sample. After spinning down the axonemes at 21130×g (15,000 rpm, FA-45-24-11 rotor, Eppendorf 5452R) for 5 min, the supernatant was desalted with the overnight dialysis against HMDEK solution (Spectra/Por Dialysis Membrane, MWCO:100-500D, Biotech CE). The concentration of the crude dynein extract was measured with Bradford method and it was around 0.02 mg/ml. High-salt extract from the demembranated axonemes contains various types of proteins [38]. Therefore, protein components of the dynein-microtubule complex should be examined with SDS-PAGEs. Spinning down the crude dynein extract with microtubules in the presence of 1mM ATP partially pulled down the outer-dynein arms and related proteins with microtubules. Using *oda1* axonemes, we repeated the same procedure on the axonemes and high-salt extracts. The resultant supernatants and pellets of the centrifugations were examined with the SDS-PAGE and the contents of *oda1* were compared with those of wild type. Inner arm dyneins, components of the central pair apparatus and radial-spoke components remain in supernatant under this condition (Fig. S1). Thus, our procedure provided ODA-DC-MT complex which contained no inner arm dyneins but only outer arm dyneins.

Negative staining electron microscopy on dynein-MT complex.

To evaluate the formation of ODA arrays on a microtubule, we examined the structure of dynein-MT complex with an electron microscope. Structural similarity of this complex to the axoneme has been reported in previous studies and was examined by negative staining electron microscopy. It showed that microtubules were periodically decorated with ODA dyneins. The crude dynein extract of 200 μg/ml was mixed with taxol-stabilized microtubules (200 μg/ml) at the various ratios (10:1, 1:1, 1:2 and 1:10). After 30-min incubation, the small aliquot of the mixture (5 μl) was applied on to a carbon grid and washed with MMEK for EM (30 mM MOPS-NaOH, 5 mM $MgSO_4$, 1 mM DTT, 1 mM EGTA, 50 mM KCl, pH 7.4). Fixation with 2% glutaraldehyde, washing with MMEK and staining with 1.4% uranyl-acetate with 100 μg/ml bacitracin. The sample was examined with JEM-1400 (JEOL, Japan) with 80kV acceleration voltage and the images of the samples were collected with 4K camera (US4000, Gatan). Typical electron micrographs are shown in Fig. S3. Coverage of the microtubules with ODA-DC complex was evaluated with image analysis. To extract the 24 nm structural repeat of dynein-ODA-DC from the electron micrographs, the custom-built band-pass filter was applied to them. The merger of the original and filtered image clearly shows the presence of dynein-DC complex. The length of the complex and microtubule length in the image field were measured.

ELASTIC MODEL

In this section we derive the relationships between the crossing angle φ, the length difference Δs and the distance

between filaments H (Fig. 3A in main text). We start with the solution derived in the main text, where the filaments shapes are described by $y_1 = A\sin kx$ and $y_2 = B\sinh kx$, with $kl = 3.9266$. The amplitude ratio is determined from the condition

$$\frac{A}{B} = \frac{\sinh kl}{\sin kl} = -0.02785\,. \tag{S1}$$

In the linear approximation, the opening angle at the pinned end is

$$\begin{aligned}\varphi &= y_1'(0) - y_2'(0) = Ak - Bk = Ak\left(1 - \frac{\sin kl}{\sinh kl}\right)\\ &= 1.02785\,Ak\,.\end{aligned} \tag{S2}$$

Also in the linear approximation, the contour length of filament i ($i = 1,2$) can be calculated as

$$s_i = \int_0^l \sqrt{1 + (y_i')^2}\mathrm{d}x \approx \int_0^l \left[1 + \tfrac{1}{2}(y_i')^2\right]\mathrm{d}x \tag{S3}$$

and the difference as

$$\begin{aligned}\Delta s &= \int_0^l \left[\tfrac{1}{2}(y_1'(x))^2 - \tfrac{1}{2}(y_2'(x))^2\right]\mathrm{d}x = \frac{lk^2}{4}(A^2 - B^2)\\ &= \frac{\sinh kl + \sin kl}{\sinh kl - \sin kl}\frac{l\varphi^2}{4} = 0.2364\,l\varphi^2\,.\end{aligned} \tag{S4}$$

Finally, we define the maximum distance between the filaments $H = \max(y_1 - y_2)$. The condition for maximality is $y_1'(x_m) - y_2'(x_m) = 0$ and leads to

$$\frac{\cos kx_m}{\cosh kx_m} = \frac{\cos kl}{\cosh kl} \tag{S5}$$

with the solution $kx_m = 1.6458$ and $H = y_1(x_m) - y_2(x_m) = 0.24301\,l\varphi$. These relationships are used in the main text to estimate the elastic energy of the two-filament system. They are also needed for the stochastic simulation.

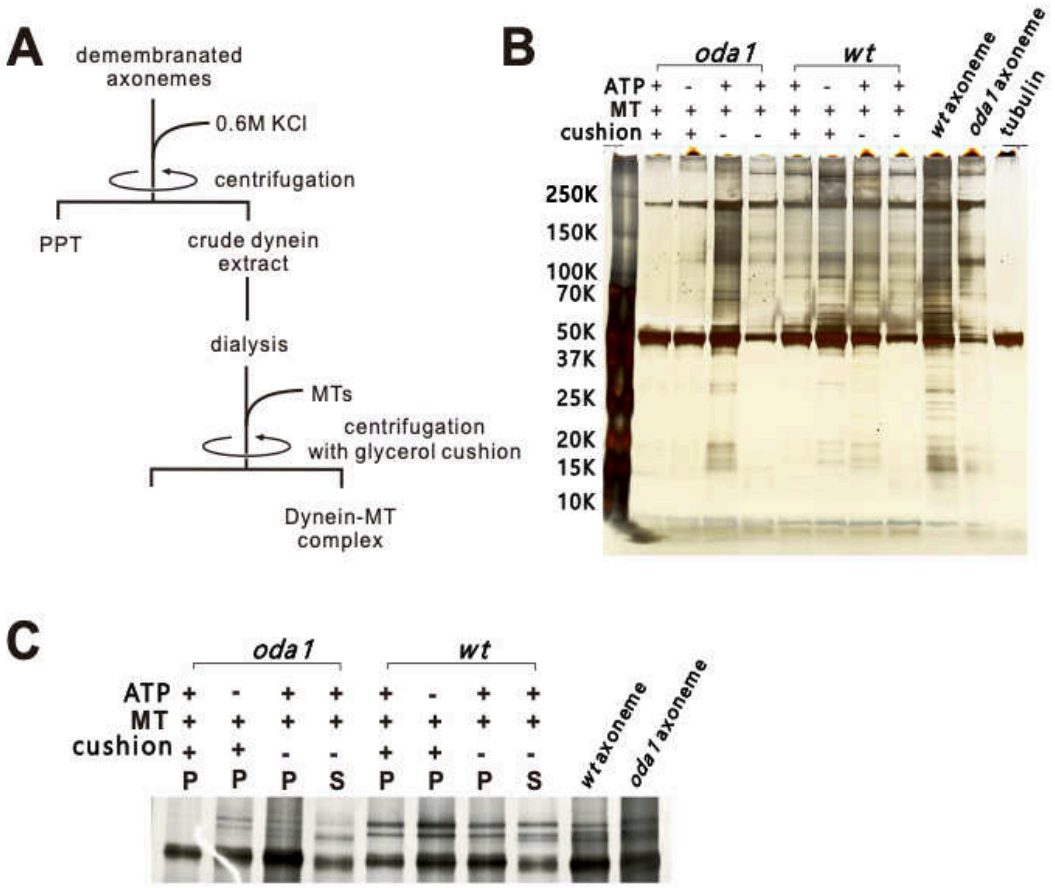

FIG. S1. Preparation of the outer-dynein arm-microtubule complex. A) Procedure of dynein-crude extraction. PPT means a precipitate B) The high-salt crude dynein extract from *Chlamydomonas reinhardtii* wild type axonemes, *oda1* axonemes and centrifuged dynein-microtubule complex were analyzed by SDS-PAGE with silver staining. Since only inner arm dyneins exist in *oda1* axonemes, the high salt extract did not contain outer arm dyneins. In contrast, the extract from wild-type axonemes contains both outer-arm dynein and inner-arm dyneins. The glycerol cushion in the centrifugation can separate inner-arm dynein from microtubules in the presence of ATP but outer arm dyneins stayed with microtubules. Lane 1: molecular weight markers. Lane 2: no dynein exists in *oda1*-extract-MT complex. No light chains and Intermediate chains of inner-arm dyneins were found. Lane 3: Removal of ATP from the complex pulled inner-arm dyneins of *oda1* extract into pellet with microtubules. Lane 4: Inner arm dyneins were found in the pellet when being centrifuged without cushion. Lane 6: Dyneins found in the pellet even in the presence of ATP and cushion but no light chains and Intermediate chains of inner-arm dyneins were found. This observation suggests that only outer arm dyneins remained on microtubules and these dyneins formed the complex with microtubules via dynein-docking complex. C) High-molecular region of 3% SDS-PAGE. Lane 1: The microtubule pellet in the presence of ATP and glycerol cushion. No dynein heavy chain was found in the pellet. Lane 2: Inner arm dynein heavy chains were found. Lane 5: Even in the presence of ATP, only outer arm dyneins were associated with microtubules. These observations suggest that our procedure enabled the ODA-DC-MT complex to contain no inner arm dyneins but only outer arm dyneins. S and P indicate a precipiate and supernatant, respectively.

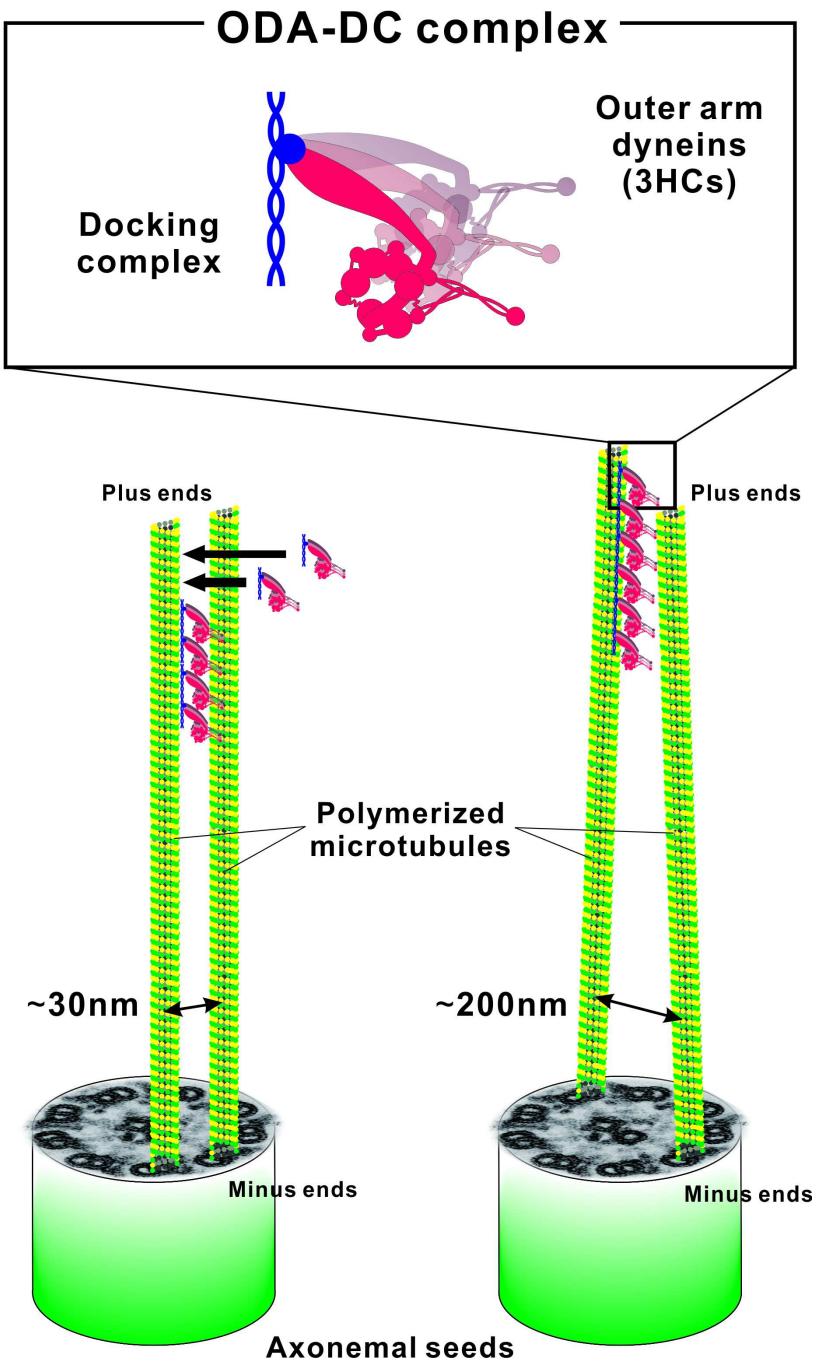

FIG. S2. Schematic representation of the assembly of a minimal synthetic axoneme with the minimal (a) and maximal (b) distance between the polymerized microtubules.

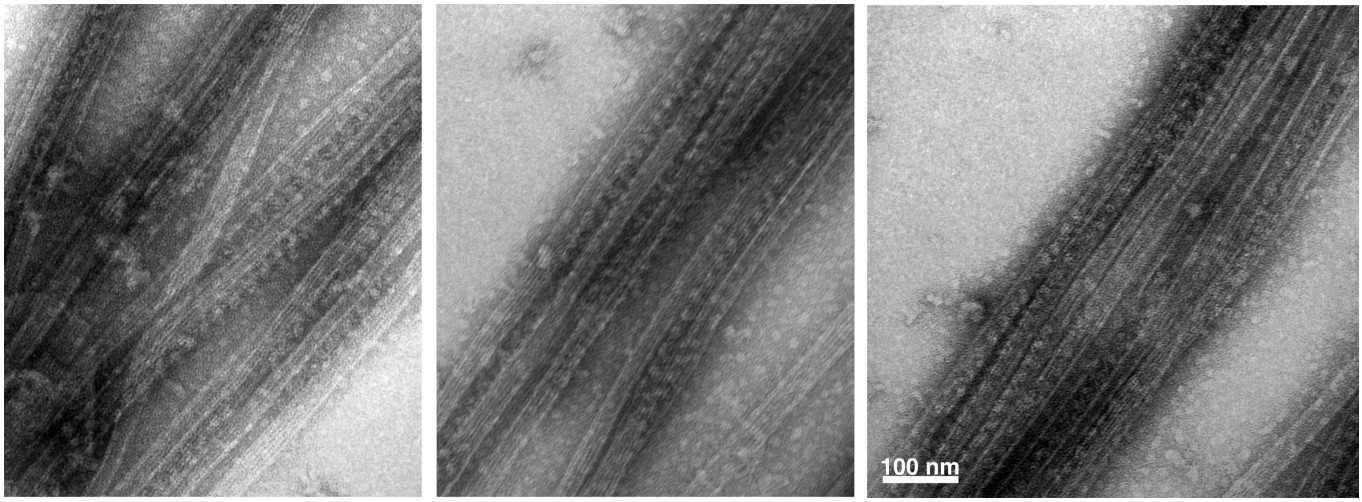

FIG. S3. Taxol-stabilized microtubules were mixed with crude dynein extract at various mixing ratios and observed with negative staining electron microscopy (acceleration voltage 80kV, magnification 25k).

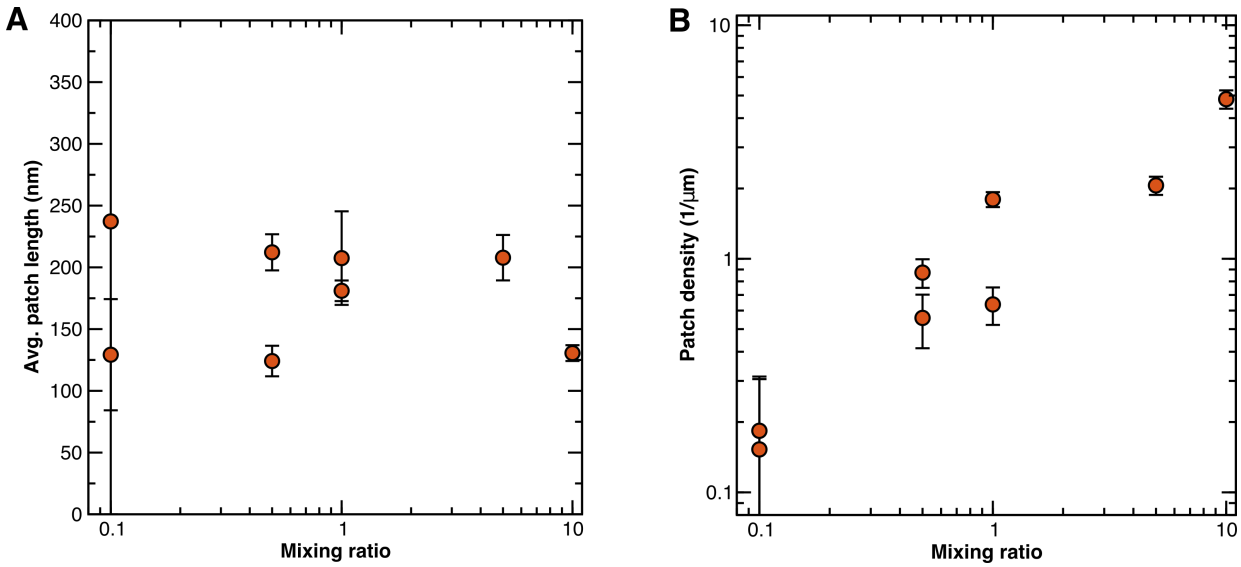

FIG. S4. Average length (A) and density (B) of dynein patches on microtubules as a function of mixing ration of crude dynein extract (4 - 400 μg/ml) to microtubules (40 μg/ml).